

FIRST PRINCIPLES STUDY OF ELECTRONIC, ELASTIC AND OPTICAL PROPERTIES OF SnO UNDER IN-PLANE BIAxIAL STRAIN

M. KASHIF^a, T. MUNIR^{a*}, N. NASIR^b, M. SHARIF^a, A. SHAHZAD^a,
T. AHMAD^c, A. HUSSAIN^a, M. NOREEN^a

^aPhysics Department, Govt College University Faisalabad (GCUF), Allama Iqbal Road, Faisalabad 38000, Pakistan

^bDepartment of Applied Sciences, Faculty of Science, National Textile University, Sheikhpur Road, Faisalabad, Pakistan

^cDepartment of Metallurgy and Materials Engineering, University of Punjab, Lahore, Pakistan

Tin mono-oxide (SnO) due to high hole and electron mobility is an excellent bi-polar oxide but due to small and indirect band gap it has limited applications for photovoltaic absorbers. In this work, we calculate the electronic properties of tensile strained SnO using full potential augmented wave method based on the density functional theory using TB-mBJ approximation. The effects of in-plane biaxial strain on electronic structure, optical property and elastic property were also investigated. The calculated band structure and density of states shows that band gap of SnO increases due to the in plane biaxial tensile strain due to weak interaction of Sn-O and Sn-Sn. A 68% increase in band gap is observed with 4% strain on SnO as compared to unstrained SnO. For elastic and optical properties, elastic constant, real and imaginary part of the dielectric function, reflectivity, absorption coefficients of unstrained and strained SnO were calculated which are in good agreement with theoretical results. This study shows that the band gap engineering of SnO can be useful for photovoltaic applications.

(Received October 13, 2018; Accepted February 15, 2019)

Keywords: First principles, Electronic properties, Elastic properties, Optical properties

1. Introduction

Tin monoxide (SnO) is a p-type semiconductor used in wide applications such as thin film transistors, photo-catalyst, inorganic solar cell and anode material for the lithium and sodium ion batteries. SnO shows 0.7 eV indirect bandgap and 2.7 eV direct bandgap. The stable phase of SnO has a layered tetragonal litharge structure (P4/nmm space group) in which one Sn atoms and four O atoms form a pyramid structure [1-4].

SnO consists of chemically inert electron pair in a hybrid $-sp$ nonbonding orbital with an electronic configuration $d^{10}s^2p^0$. This inert electron pair called lone pairs is directed towards the interlayer separation. The electron charge clouds of Sn-5s states screen the positive charges on Sn²⁺ ions in SnO, which do not contribute in the bonding. The lone pair states affect the band

*Corresponding author: tariqmunir@gcuf.edu.pk

structure of the SnO. Inter-layer Sn-Sn distance changes can change the role of lone pair interactions [5-12].

Band gap tuning can be achieved by changing the inter layer interaction. Furthermore, the band structure strained SnO has not been yet theoretically discussed in detail. We study the response of the SnO band structure, optical and elastic properties when subjected to biaxial strain to improve the electrical performance of SnO for transparent electronic device applications.

2. Methodology

The structural optimization of SnO was performed with Quantum Espresso code based on density functional theory. Perdew-Wang 1991 (PW-91) functional with Generalized Gradient Approximation (GGA) was used for the structural optimization. Ultrasoft pseudopotentials was used for Sn and O ions cores. The plane wave cutoff energy was 60 Ry and the Brillion-zone integration was performed over the $8 \times 8 \times 6$ grid sizes using the Monkhorst –Pack method for SnO structure optimization. Broyden-Fletcher-Goldfarb-Shenno (BFGS) minimization technique was used for the structural optimization. Convergence criteria for geometry optimization was 10^{-6} au for the energy and of 10^{-3} au for the forces per atom. The in-plane biaxial strain is defined by

$$\varepsilon_a = \frac{a - a_0}{a_0}$$

where a_0 is optimized in-plane lattice constant for the unstrained case and a is

the in-plane lattice constant for the strained case. In this study only the tensile strained was study.

The electronic, elastic and optical properties of strained SnO was calculated using the full-potential linearized augmented plane waves (FLAPW) method implemented in WIEN2K. The exchange correlation potential is in the form of TB-mBJ which gives the band gap close to experimental values. The convergence of the basis set is controlled by a cutoff parameter $\text{RMT} \times K_{\text{max}} = 7$, where K_{max} is magnitude of the largest K vector. The radius of muffin–tin (RMT) sphere values for Sn and O atoms were taken to be 2.1 and 1.9 a.u respectively. Self- consistent calculations were done with 1000K points in the full Brillouin zone and total energy is converged to within 0.0001Ry.

3. Results and discussion

Fig.1 shows tetragonal litharge-type crystal structure of tin monoxide (SnO) (space group = P4/nmm, No. 129). The position of oxygen atoms are (0,0,0) and (0.5a,0.5a,0) while the position of Sn atoms are (0, 0.5a,uc) and (0.5a, 0, -uc) with $u = 0.238$. Geometry optimization was carried out to calculate the lattice parameter of SnO. The calculated lattice parameters are $a = b = 3.84 \text{ \AA}$ and $c = 4.91 \text{ \AA}$, which are close to the experimental data ($a = b = 3.80 \text{ \AA}$ and $c = 4.84 \text{ \AA}$) [13]. Then we use these optimized lattice parameters for the calculation of strained lattice parameter using

$$\varepsilon_a = \frac{a - a_0}{a_0}$$

The increase in the bond length of Sn-O and Sn-Sn is observed with increase in the

biaxial strain.

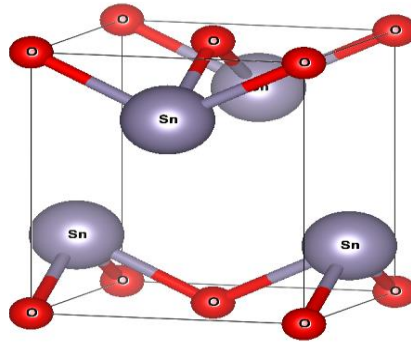


Fig.1. SnO litharge-type tetragonal structure.

Table 1. Bond length of SnO under different strains.

	Sn-O	Sn-Sn
0%	2.2452	3.7602
2%	2.2783	3.7997
4%	2.3115	3.8396

3.1. Electronic properties

To study the effects of strain on the electronic properties of SnO, the band structures plots under different strains are shown in Fig. 2. It is observed that with increasing the tensile strain, the conduction band minima (CBM) shifts upward and the indirect gap character of SnO is still maintained, and it shows tunable bandgap under strain. Fig.2 (a) shows that valence band maxima (VBM) rests at gamma point, while on other hand conduction band minima (CBM) rests at M point and the energy band gap is computed along gamma to M symmetry points. The dotted line between VBM and CBM denoted to the Fermi level, which is selected to be at zero energy level. The calculated band gap along these symmetry points is 0.686 eV and it implies that SnO is an indirect band gap semiconductor, which is very close to the experimental value of 0.7eV. While on other hand, in the presence of strain effect, the high symmetry points along which we calculated the band gap at VBM and CBM remain unchanged but the value of band gap increased up to 1.154 eV with increasing strain ratio, which is clearly shown in Fig. 2 (b) and (c). It implies that the magnitudes of band gap of SnO can be varied by operating different ratios of tensile strain. The band gap opening is due to the weak interaction of Sn-O and Sn-Sn [6]. The bond length increases as with increase in the in-plane biaxial strain Sn-O and Sn-Sn shown in Table.1. Further, it is observed that the conduction band minimum is dispersed along (X-r-M) direction and conduction band minimum is doubly degenerate. The valance band edge along the r-M has low dispersion and high dispersion along the r-Z direction. The valance band structure shows small hole effective masses in SnO which is the important characteristics of the p-type transistor to achieve the high hole mobility [14].

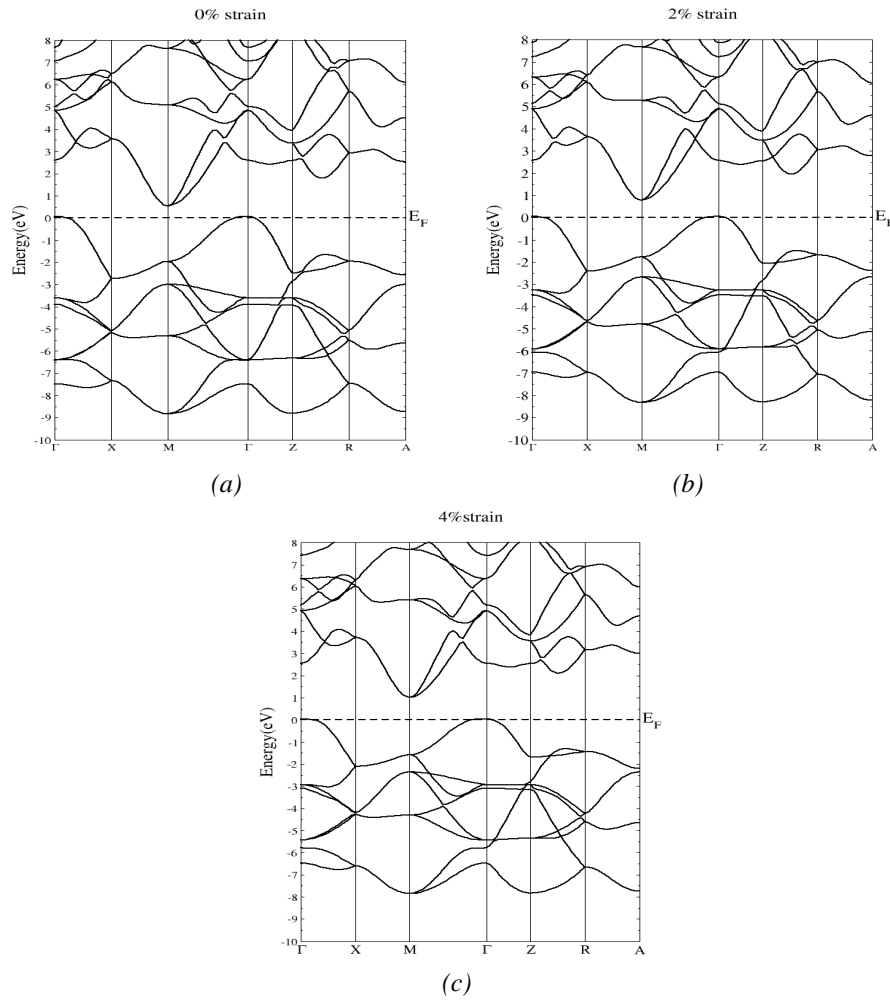


Fig. 2. Band structure at (a) 0% (b) 2% and (c) 4%.

In order to know the strain effect on DOS, we plot the total DOS plots of SnO under different strains shown in Fig. 3. From total DOS plots, we clearly see that the lower edge of valence band moves towards higher energy range by increasing tensile strain, also same trend is observed for the upper part. With increasing the in-plane biaxial tensile strain, the energy gap between VBM and CBM also increases.

Fig.4 shows Partial density of states (PDOS) which provides the deep understanding of the electronic structure. It is observed that the top of the valence band from the energy range 0 to -3eV is composed of Sn-5s and Sn-5p states and O-2p state, this region represents the anti-bonding character. The region from the top of valence band represents the bonding character due to Sn-5s and O-2p hybridization. The region between the energy -3eV to -6.5 eV O-2p state is dominated with small contribution from the Sn-s and Sn-p states. The conduction band maximum is mainly composed of Sn-p and O-p states. The strong hybridization between the O-2p and Sn-5s states exist and Sn-s lone pair electrons interact with the O-p state. This shows that intra-layer role from the lone pair to the bonding is significant.

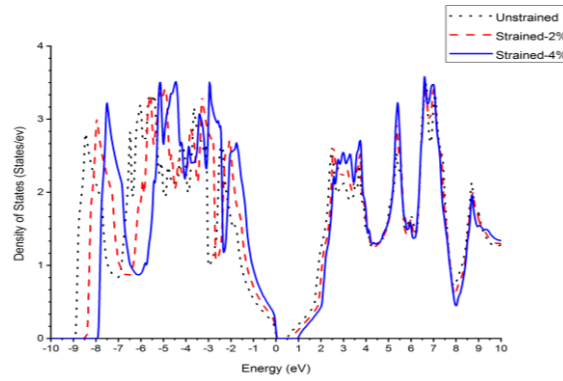


Fig.3. Total density of states for SnO under different strains.

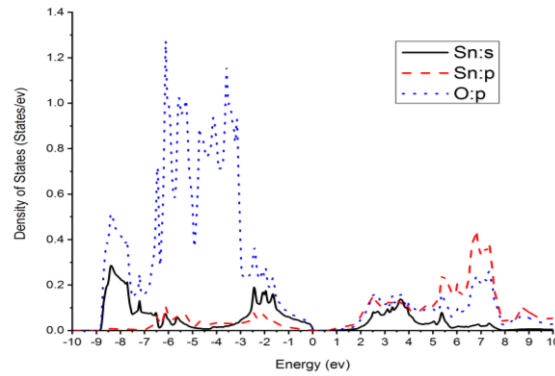


Fig.4. Partial density of states for SnO

3.2. Elastic properties

In the materials, the elastic constants C_{ij} always play a very useful role in determining the strength. In relation to the elastic constants, we can find the stiffness, stability, brittleness, ductility, bulk modulus, Young's modulus, shear modulus and anisotropy knowledge of the materials.

The mechanical stability conditions for tetragonal phase checked by Born stability criteria. For tetragonal symmetry, we check the mechanical stability of structure by following elastic stiffness constants conditions [3-4,15-16].

$$C_{11} > 0, C_{33} > 0, C_{44} > 0 \text{ and } C_{66} > 0$$

$$C_{11} - C_{12} > 0 \text{ and } C_{11} + C_{33} - 2 C_{13} > 0$$

$$(2 C_{11} + C_{33} + 2 C_{12} + 4 C_{13}) > 0 \quad (1)$$

The calculated crystal elastic constants C_{ij} of SnO under biaxial strain are listed in Table.2. It is clearly indicated that the calculated elastic constants of tetragonal phase SnO in our calculation confirm these mechanical stability conditions, overall, all individual elastic constants are greater than zero. We noted that the values of elastic constants C_{12} and C_{13} are gradually increases by increasing tensile strain ratio and C_{66} gradually reduced by enhancing strain ratio,

while the values of C_{11} , C_{33} and C_{44} are fluctuates by increasing strain ratio. It is observed that $C_{11} > C_{33}$ which shows that the bonds are stronger in the [100] and [010] direction as compare to bonds along [001] direction. Also it is observed that when $C_{44} < C_{66}$ it shows that in [100] direction and (010) plane, shear is more difficult than the [100] direction and (001) plane.

Table 2. The elastic constants C_{ij} (GPa).

	C_{11}	C_{12}	C_{13}	C_{33}	C_{44}	C_{66}
Ref [4]	147.8	83.9	53.4	102.2	43.9	75.6
Ref [3]	92	83	24	35	21	72
0%	183.3	47.36	47.30	84.24	23.86	80
2%	123.52	87.46	63.77	102.51	27.18	64
4%	250	219.25	116.32	79	24.21	27

The Voigt-Reuss-Hill approximation was used to calculate the bulk modulus B and shear modulus G. The relevant elastic tensors B_V , B_R , B, G_V , G_R and G with different strains are given in the Table-3. The ratio of bulk to shear modulus B/G is used for the determination of ductile and brittle character. The bulk modulus B represents the resistance to volume change while the shear modulus G characterizes the resistance to plastic deformation. High value of B/G ratio shows the ductile property of the materials, whereas a low value shows the brittle property. If $B/G > 1.75$, the material shows the ductility otherwise, the material shows brittle property. The ratio B/G also shows the hardness of a material. Hardness of the material has high value when B/G ratio is low. The elastic tensors calculated together with bulk, shear, Young's modulus and Poisson ratio under different biaxial strains are presented in Table-3. It is observed that all the elastic modulus decrease linearly at different rates with increased tensile strains except bulk modulus which is increases with strains. The bulk modulus represents the resistance to change in volume. Therefore, with increase in strain it is observed that bulk modulus increase which shows that it is difficult to change in the volume of SnO crystal with strains. The effect of biaxial strains on the ductility or brittleness can be calculated. The ratio B/G represents the ductility or brittleness of the crystal. From the Table-3 it is observed that B/G ratio is greater than 1.75 and increases with different strains which shows that SnO behave ductile manner.

Table. 3. Bulk modulus, B (GPa), shear modulus, G (GPa), Young's modulus, Y (GPa), and Poisson ratio, ν , of SnO under different strains.

	B_V	B_R	B	G_V	G_R	G	Y	ν
0%	81.64	71.24	76.44	40.8	34.78	37.78	97.33	0.42
2%	86.61	109.13	97.86	32.57	28.74	30.65	83.26	0.36
4%	164.75	61.8	113.27	23.56	17.64	20.59	58.26	0.41

Anisotropy indexes, the compression and shear anisotropic factors (A_B , A_G) are used to find the anisotropy in elasticity which can be obtained from the following equations

$$A_B = \frac{B_v - B_R}{B_v + B_R} \quad (2)$$

$$A_G = \frac{G_v - G_R}{G_v + G_R} \quad (3)$$

Anisotropic factors value represents varying degrees of anisotropy when value is less than greater than zero. Anisotropic factors value equal to zero shows that crystal has isotropic properties. Shear modulus anisotropy is smaller than the bulk modulus anisotropy. Biaxial strains have more effect on the bulk modulus anisotropy, which means that SnO seems to be more anisotropic under compression than in shear as shown in the Table 4.

Table. 4. Anisotropic constants of SnO as a function of strains.

	A_B	A_G
0%	0.06	0.07
2%	-0.11	0.06
4%	0.45	0.14

3.3. Optical properties

In crystal structure, the transition of electrons for optical properties relate to frequency dependent complex dielectric function $\varepsilon(\omega) = \varepsilon_1(\omega) + i\varepsilon_2(\omega)$. The imaginary part ($\varepsilon_2(\omega)$) of the complex dielectric function is computed from the momentum matrix elements between occupied ($\psi_v(\vec{k})$) wave function and unoccupied ($\psi_c(\vec{k})$) wave function [17-20].

$$\varepsilon_2(\omega) = \left(\frac{e^2 2\pi}{\Omega \epsilon_0} \right) \sum \left| \langle \psi_c(\vec{k}) | u \times r | \psi_v(\vec{k}) \rangle \right|^2 \delta(E_k^c - E_k^v - E) \quad (4)$$

where the integral is over the first Brillouin zone, e and ω symbolize the electronic charge and light frequency respectively. From dispersion transition probability and Kramer Kronig relation, the real part $\varepsilon_1(\omega)$ of complex dielectric function is calculated from the imaginary part. The other optical properties are calculated using these relations.

$$\alpha(\omega) = \sqrt{2\omega} [\sqrt{\varepsilon_1^2(\omega) + \varepsilon_2^2(\omega)} - \varepsilon_1(\omega)]^{1/2} \quad (\text{for absorption}) \quad (5)$$

$$R(\omega) = \left| \frac{\sqrt{\varepsilon_1(\omega) + i\varepsilon_2(\omega)} - 1}{\sqrt{\varepsilon_1(\omega) + i\varepsilon_2(\omega)} + 1} \right| \quad (\text{for reflectivity}) \quad (6)$$

The imaginary part of dielectric function from band structure can be directly obtained through all electron method (WEIN2k) and the real part can be computed with the help of transition probability and Kramer Kronig relations. For the study of optical transition, the imaginary part is a key parameter. Considering the tetragonal litharge structure, the optical properties of SnO have anisotropic with crystallographic c-axis. In this way, the unstrained and strained imaginary part graphs of SnO in [100] and [001] direction are shown in Fig. 5. Imaginary part of the dielectric function represents the electron excitation which is observed in term of peaks. The main peaks, as seen in unstrained SnO have a four primarily peaks close to the photon energy 3.5eV, 4.7eV, 7.7eV and 8.7eV. Electrons transitions corresponding to the peaks obtained in imaginary plot are analyzed according to transition law and value of peak which matches transition energy.

The peak of 3.5 eV is attributed to the transition between O-2p in the VBM and Sn-5s in CBM. Interband transition of the O 2p to Sn 5s is related to peaks of 4.7 eV and 7.7 eV. And the peak of 8.7 eV is related with the transition of the Sn 5p to O-2s. In both directions, by increasing biaxial strain the energy peaks shift toward higher energy and it shows the blue shift phenomena.

The real part of the calculated dielectric function for unstrained and strained of SnO in [100] and [001] direction is shown in Fig. 6. For the unstrained SnO the static value ($\omega=0$) of dielectric constant $\epsilon_{[100]}(0) = 6.2$ for 2% and 4% strained SnO are $\epsilon_{[100]}(0) = 6.1$ and $\epsilon_{[100]}(0) = 6.0$, it means that, in [100] direction, the values of dielectric constant decreases by increasing strain ratio. For [001] direction, the value of static dielectric constant of unstrained and strained SnO is around 5, It implies that, the strain has only effect the value of dielectric constant of anisotropic crystal structure for polarization vector [100].

For optoelectronic devices, the absorption spectrum key parameter to estimates the optical behavior of materials. The absorption spectra of unstrained and strained of both along [100] direction and [001] direction are presented in Fig. 7. We noted that the absorption peak maxima of unstrained SnO along [001] direction is found at comparatively higher energy value than that of [100] polarization vector. With the increase in biaxial strain it is observed that in [001] direction the absorption spectra shift towards lower energy and in [100] direction spectra shift towards higher energy. Furthermore, it is observed that, in visible energy region the absorption of unstrained and strained SnO along polarization vector [100] is greater than that of parallel to c-axis. It means that along [001] direction, the SnO is more transparent as compared to [100] direction.

The reflectivity behavior of pure and strained SnO along parallel and perpendicular to crystallographic c-axis are shown in Fig. 8. We observed that in low energy region (visible region) along [001] direction the reflectivity rate of electromagnetic radiations is higher than of [100] polarization vector but overall low reflectivity observed from SnO in both parallel and perpendicular to c axis.

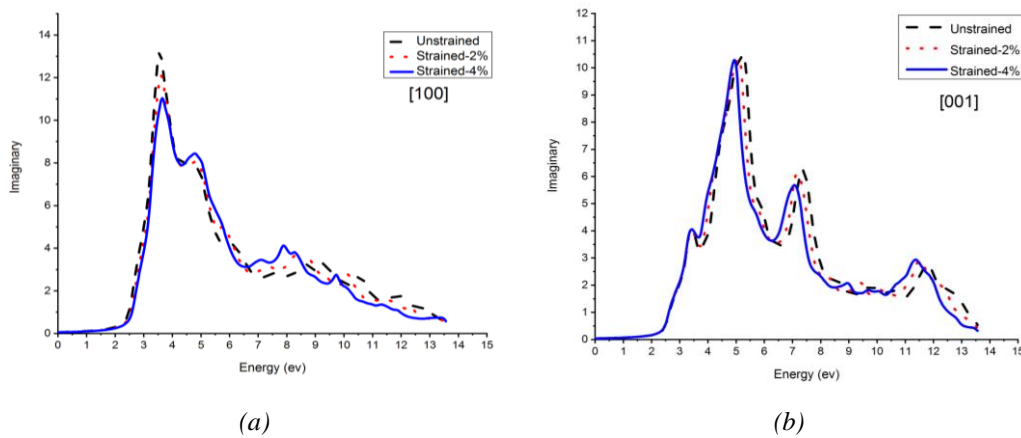


Fig.5. Imaginary part of the dielectric functions along (a) [100] and (b) [001] directions under different strains.

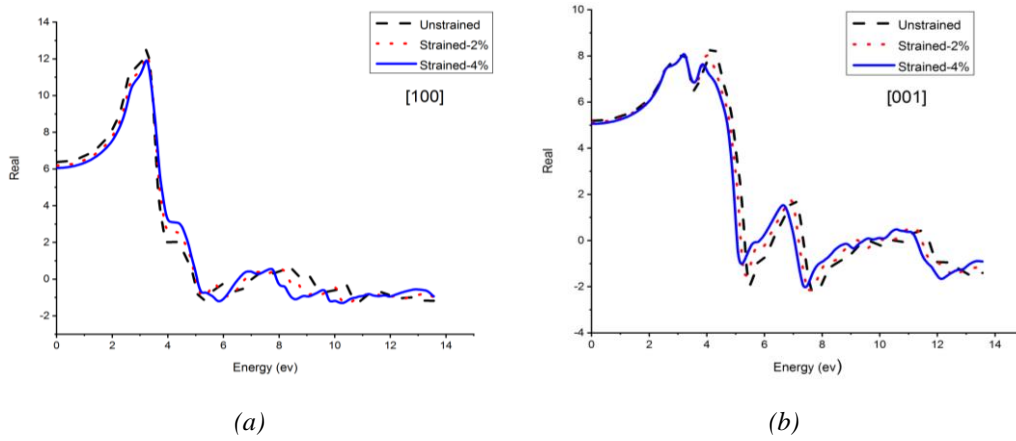


Fig.6. Real part of the dielectric functions along (a) [100] and (b) [001] directions under different strains.

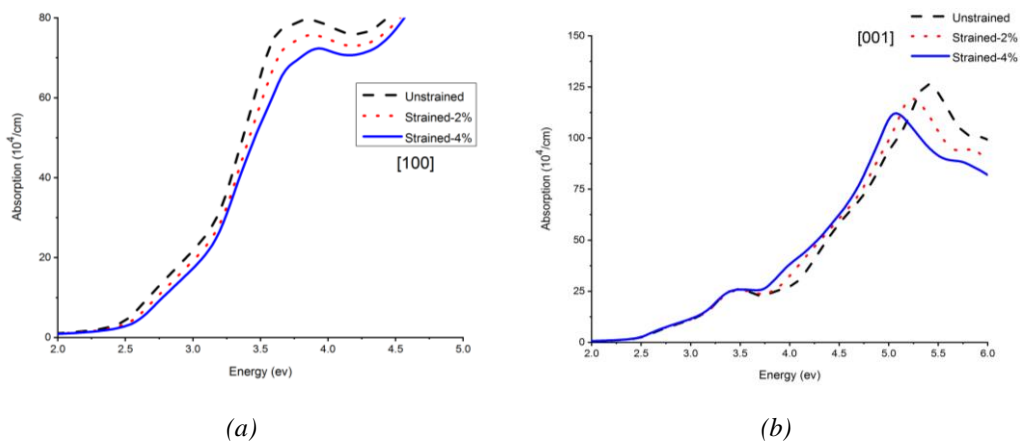


Fig.7. Absorption coefficient along (a) [100] and (b) [001] directions under different strains.

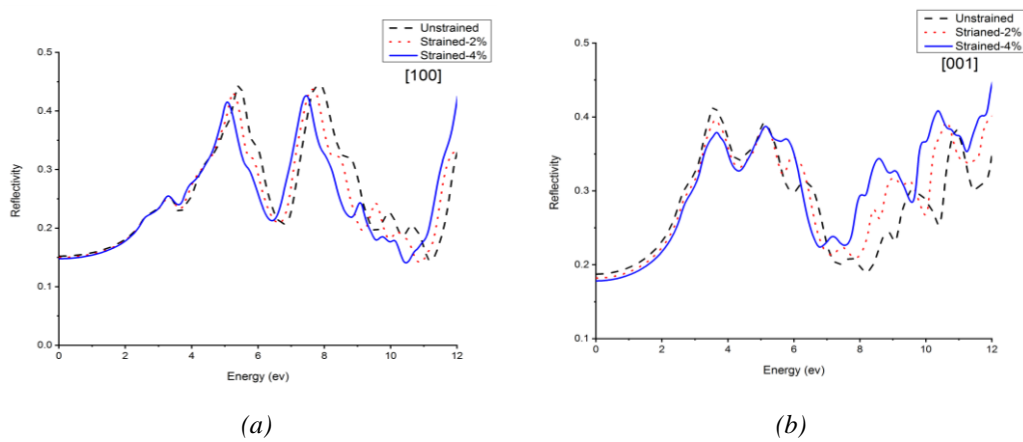


Fig.8. Reflectivity along (a) [100] and (b) [001] directions under different strains.

4. Conclusions

The effect of in-plane biaxial strain on SnO has been investigated. It was found that band gap increases linearly with the increase in in-plane biaxial strain which mainly comes from the role of Sn-O and Sn-Sn interaction. Dielectric constant decreases with increase in the strain. Blue shift in optical properties is observed with increase in the strain in [100] direction. Hence, we can change the physical properties of SnO with the biaxial strain and thus allows a number of significant technological applications in optoelectronics.

Acknowledgements

The computational facilities for this work were provided by Department of Physics, Govt College University Faisalabad.

References

- [1] Q. J. Liu, Z. T. Liu, L. P. Feng, *Computational Materials Science* **47**(4), 1016 (2010).
- [2] J. Du, C. Xia, Y. Liu, X. Li, Y. Peng, S. Wei, *Applied Surface Science* **401**, 114 (2017).
- [3] M. A. Ali, A. K. M. A. Islam, N. Jahan, S. Karimunnesa, *International Journal of Modern Physics B* **30**(31), 1650228 (2016).
- [4] I. Erdem, H.H. Kart, T. Cagin, *Archives of Materials Science and Engineering* **45**(2), 108(2010).
- [5] J. P. Allen, D. O. Scanlon, L. F. Piper, G. W. Watson, *Journal of Materials Chemistry C* **1**(48), 8194 (2013).
- [6] H. Peng, A. Zakutayev, S. Lany, Tuning optical absorption of SnO by isoelectronic alloying for PV absorber, 1504 (2015).
- [7] J. M. Raulot, G. Baldinozzi, R. Seshadri, P. Cortona, *Solid state sciences* **4**(4), 467 (2002).
- [8] N. E. Christensen, A. Svane, E. P. Blacá, *Physical Review B* **72**(1), 014109 (2005).
- [9] S. A. Miller, P. Gorai, U. Aydemir, T. O. Mason, V. Stevanović, E. S. Toberer, G. J. Snyder, *Journal of Materials Chemistry C* **5**(34), 8854 (2017).
- [10] W. Zhou, N. Umezawa, *Physical Chemistry Chemical Physics* **17**(27), 17816 (2015).
- [11] A. Walsh, D. J. Payne, R. G. Egdell, G. W. Watson, *Chemical Society Reviews* **40**(9), 4455 (2011).
- [12] J. Köhler, J. Tong, R. Dinnebier, A. Simon, *Zeitschrift für anorganische und allgemeine Chemie* **638**(12-13), 1970 (2012).
- [13] P. J. Chen, H. T. Jeng, *Scientific reports* **5**, 16359 (2015).
- [14] C. W. Shih, A. Chin, C. F. Lu, W. F. Su, *Scientific reports* **8**(1), 889 (2018).
- [15] H. Zhai, X. Li, J. Du, *Materials transactions* **53**(7), 1247 (2012).
- [16] O. Beckstein, J. E. Klepeis, G. L. W. Hart, O. Pankratov, *Physical Review B Phys Rev B* **63**, 13411 (2016).
- [17] Y. Zhao, H. Yang, B. Yang, Z. Liu, P. Yang, *Solar Energy* **140**, 21 (2016).
- [18] L. Peng-Fei, S. Yue, Y. Zhong-Yuan, Z. Long, L. Qiong-Yao, M. Shi-Jia, L. Yu-Min,

- Communications in Theoretical Physics **57**(1), 145 (2012).
- [19] P. D. Borges, L. M. Scolfaro, H. W. L. Alves, E. F. da Silva, Theoretical Chemistry Accounts **126**(1-2), 39(2010).
- [20] D. Guo, C. Hu, Applied Surface Science **258**(18), 6987 (2012).